Kidney Diseases

Research Article

Kidney Dis 2022;8:408–423
DOI: 10.1159/000526139

Received: February 22, 2022
Accepted: July 8, 2022
Published online: September 27, 2022

KYA1797K, a Novel Small Molecule Destabilizing β-Catenin, Is Superior to ICG-001 in Protecting against Kidney Aging

Mingsheng Zhu[a, b] Xian Ling[a] Shan Zhou[a] Ping Meng[c] Qiyan Chen[d] Shuangqin Chen[a] Kunyu Shen[a] Chao Xie[d] Yaozhong Kong[d] Maosheng Wang[e] Lili Zhou[a]

[a]State Key Laboratory of Organ Failure Research, National Clinical Research Center of Kidney Disease, Guangdong Provincial Key Laboratory of Renal Failure Research, Division of Nephrology, Nanfang Hospital, Southern Medical University, Guangzhou, China; [b]Department of Nephrology, The People's Hospital of Gaozhou, Maoming, China; [c]Department of Nephrology, Huadu District People's Hospital, Southern Medical University, Guangzhou, China; [d]Department of Nephrology, The First People's Hospital of Foshan, Foshan, China; [e]The Cardiovascular Center, The People's Hospital of Gaozhou, Maoming, China

Keywords
KYA1797K · Mitochondrial dysfunction · Kidney aging · β-Catenin · ICG-001

Abstract
Introduction: Aged kidney is characterized by mitochondrial dysfunction, cellular senescence, and fibrogenesis. The activation of Wnt/β-catenin signaling plays an important role in the initiation of kidney aging. However, the inhibiting strategies have not been discovered in detail. Here, we compared the therapeutic effects of two β-catenin inhibitors, KYA1797K and ICG-001, to assess their superiority. ***Methods:*** Two-month-old male C57BL/6 mice which had undergone unilateral nephrectomy and received D-galactose (D-gal) injection were co-treated with KYA1797K or ICG-001 at 10 mg/kg/day for 4 weeks. Human proximal renal tubular cells were treated with D-gal and KYA1797K/ICG-001 to compare their effects. ***Results:*** Compared with ICG-001, which inhibits β-catenin pathway through blocking the binding of β-catenin and cAMP response element-binding protein (CREB)-binding protein (CBP), KYA1797K, a novel small molecule destabilizing β-catenin through activating Axin-GSK3β complex, possesses the superior effects on protecting against kidney aging. In D-gal-treated accelerated aging mice, KYA1797K could greatly inhibit β-catenin pathway, preserve mitochondrial homeostasis, repress cellular senescence, and retard age-related kidney fibrosis. In cultured proximal tubular cells, KYA1797K shows a better effect on inhibiting cellular senescence and could better suppress mitochondrial dysfunction and ameliorate the fibrotic changes, at the same dose as that in ICG-001. ***Conclusion:*** These results show that effectively eliminating β-catenin is a necessity to target against age-related kidney injury, suggesting the multiple transcriptional regulation of β-catenin in kidney aging besides T-cell factor/lymphoid enhancer-binding factor family of transcription factors (TCF/LEF-1).

Introduction

The kidney is one of the most important organs to maintain the water-and-electrolyte balance and keep the stability of metabolic state [1–3]. Aging has a positive correlation with estimated glomerular filtration rate loss and urinary albumin (Ualb) leaking [4]. Many factors, such as persistent inflammation and nutrient insensitivity in ag-

Karger@karger.com
www.karger.com/kdd

Correspondence to:
Maosheng Wang, mmwmsmd@126.com
Lili Zhou, jinli730@smu.edu.cn

ing could lead to kidney injury [5–8]. Notably, the kidney is the most abundant organ with Klotho [9], an antiaging protein which modulates life span through its beneficial effects [10–12]. We have found that Klotho also acts as an endogenous inhibitor to Wnt/β-catenin signaling [9], an important player in kidney aging and renal tubular senescence [13, 14].

Cellular senescence is a permanent state of irreversible cell cycle arrest resulting from a variety of stresses [15–17]. It can be induced by a variety of factors, including telomere shortening, telomere dysfunction, DNA damage, inflammation, mitochondrial dysfunction, epigenetic disruption, and strong mitogen signaling or oncogenes [18, 19]. Senescent cells are causally involved in aging. The persistent presence of senescent cells may secrete multiple factors including cytokines or chemokines, proteases, ROS, and microRNAs, which further cause inflammation, tissue fibrosis, and stem cell dysfunction, resulting in the dysfunction of multiple organs and accelerated aging [19–21]. Characterized with cellular senescence, mitochondrial dysfunction, and age-related fibrosis, kidney aging is highly accompanied by the activation of Wnt/β-catenin signaling [13]. β-Catenin is the downstream effector of Wnt signals, which is able to translocate into the nucleus and bind to the T-cell factor (TCF)/lymphoid enhancer-binding factor (LEF) family of transcription factors [22, 23]. cAMP response element-binding protein (CREB)-binding protein (CBP) is a co-activator which enhances the binding of β-catenin and TCF/LEF-1 [24]. ICG-001 is a small molecule compound which inhibits β-catenin pathway through blocking the binding of β-catenin and CBP [25]. Although the β-catenin/TCF/LEF-1 pathway induces multiple targets involved in fibrogenesis [22, 26], its role in kidney aging has not been elucidated. Considering the multiple downstream transcription factors which could be activated by β-catenin, such as the forkhead box O (FOXO) protein family as reported recently [27–29], β-catenin could trigger a variety of pathways to cooperatively accelerate aging processes in kidneys. Hence, a better strategy to eliminate β-catenin would be more beneficial.

In normal conditions, β-catenin would be phosphorylated at the site of Ser/Thr-rich sequence near the amino terminus and ubiquitinated by the "destruction complex," which includes Axin, adenomatous polyposis coli (APC), GSK3β, CK1, PP2A, and β-TrCP, an E3-ubiquitin ligase [30]. In this process, Axin is a requisite for the scaffolding of β-catenin and other kinases [31]. The ubiquitinated β-catenin is then degraded by proteasome, which means that ubiquitin-dependent proteolysis system is involved in the regulation of β-catenin. Without Wnt signal, the phosphorylation of β-catenin by GSK3β would represent the initial event for ubiquitination and degradation of β-catenin [32]. While upon the stimulation of Wnt, β-catenin will be dephosphorylated and accumulate in the cytoplasm and then translocate into nuclei to induce the transcription of downstream targets [33]. Hence, the strategies to enhance the degradation of β-catenin would be ideal for targeted inhibition of the aberrant upregulation of β-catenin. Interestingly, the recent report shows KYA1797K, a small molecule compound which could induce the destabilization of β-catenin via binding to Axin and activating the destruction complex function [34]. However, the effects of KYA1797K on kidney aging have not been clarified.

In this study, we testified the therapeutic effects of KYA1797K on D-galactose (D-gal)-induced accelerated aging mice model and cultured human proximal renal tubular cells. We also compared the therapeutic effects of two β-catenin inhibitors, KYA1797K and ICG-001, to assess their superiority. The results show that KYA1797K, the β-catenin destructor, exhibits the superior effectiveness in maintaining mitochondrial homeostasis and restraining kidney aging. Considering ICG-001 functions mainly through the inhibition of β-catenin/TCF/LEF-1-mediated targets transcription, we believe that effectively eliminating β-catenin is a more ideal strategy to target the aberrantly activated β-catenin signaling in kidney aging, since other downstream transcription factors would also be possibly involved.

Material and Methods

Animal Models

Male C57BL/6 mice (2 and 24 months old) were purchased from the Experimental Animal Center of Southern Medical University (Guangzhou, China). For comparison with 24-month-old mice, 2-month-old mice were sacrificed without any special treatment. For the accelerated aging mice model, unilateral nephrectomy was performed in the 2-month-old mice first and then D-gal (G0750; Sigma-Aldrich, USA) at 150 mg/kg/day was injected subcutaneously into the mice for 6 weeks from 1 week after the surgery. The KYA1797K (s8327; Selleck, USA) or ICG-001 (847,591-62-2; ChemLeader, China) at 10 mg/kg/day was injected intraperitoneally in the mice every day for 4 weeks after 2 weeks' injection of D-gal. The detailed experimental designs were shown in indicated Figure. All animal experiments were approved by the Animal Ethics Committee at Southern Medical University.

Cell Culture and Treatment

Human proximal tubular epithelial cells (HKC-8) were provided by Dr. L. Racusen (Johns Hopkins University, Baltimore, MD, USA). To assess the effects of ICG-001 and KYA1797K on

β-catenin, the HKC-8 cells were treated with ICG-001 or KYA1797K at the concentration of 1 μM for 60 h. To assess the effects on cellular senescence, fibrosis, and mitochondrial dysfunction, HKC-8 cells were pretreated with ICG-001 or KYA1797K at 1 μM for 1 h, followed by treatment with D-gal at 10 mg/mL for 60 h. The lysates of the cells were subjected to Western blot analyses. Besides, cells cultured on the coverslips were also assessed by immunofluorescence.

Western Blot Analysis

The kidney tissue or cultured cells were dissolved in the lysis buffer, and the concentrations of proteins were measured using BCA protein concentration determination. Then the proteins were transferred to a PVDF (polyvinylidene fluoride) membrane (Merck Millipore, USA) by SDS-PAGE electrophoresis and blocked with skim milk for 1 h, followed by incubation with primary antibodies overnight at 4°C and with secondary antibodies for 1 h at room temperature in the next day. An ECL kit (Applygen, China) was used for visualizing the antigen-antibody complexes. The primary antibodies used were as follows: anti-fibronectin (1:20,000; F3648, Sigma-Aldrich), anti-GAPDH (1:20,000; RM2001, Ray Antibody Biotech, China), anti-β-catenin (1:30,000; #610154, BD Transduction Laboratories, USA), anti-PGC-1α (1:1,000; ab54481, Abcam, UK), anti-Klotho (1:1,000; AF1819, R&D Systems, USA), anti-α-smooth muscle actin (α-SMA) (1:3,000; a2547, Sigma-Aldrich), anti-α-SMA (1:1,000; ab5694, Abcam), anti-TFAM (1:1,000; PB0413, Boster, USA), anti-active β-catenin (1:1,000; 19807s, Cell Signaling Technology, USA), anti-$p16^{INK4A}$ (1:1,000; ab189034, Abcam), anti-$p19^{ARF}$ (1:1,000; ab26696, Abcam), anti-γH2AX (1:1,000; ab26350, Abcam), anti-TOMM20 (1:2,000; ab186735, Abcam), anti-BAX (1:500; sc-7480, Santa Cruz Biotechnology, USA), anti-cleaved PARP-1 (1:1,000; 9542s, Cell Signaling Technology), anti-cleaved caspase-3 (1:500; 9661s, Cell Signaling Technology), anti-FAS-L (1:500; sc-19681, Santa Cruz Biotechnology), and anti-α-tubulin (1:10,000; RM2007, Ray Antibody Biotech).

Histology, Immunohistochemical Staining, and Transmission Electron Microscopy

Paraffin-embedded kidney sections (3 μm thickness) were prepared for Sirius red staining (DC0040; Leagene Biotechnology, China) according to the manufacturer's protocol to assess renal fibrosis. Immunohistochemical staining was performed using routine protocol to assess mitochondrial function, renal fibrosis, or renal senescence. Images were taken by the DP27-CU camera coupled to BX-43F microscope (Olympus, Japan). The primary antibodies used were as follows: anti-$p16^{INK4A}$ (1:100; ab189034, Abcam), anti-PGC-1α (1:80; ab54481, Abcam), anti-fibronectin (1:100; F3648, Sigma-Aldrich). In order to assess the mitochondrial morphology by transmission electron microscopy (TEM), the cortex of the kidney was fixed in 1.25% glutaraldehyde/0.1 M phosphate buffer and then made into ultrathin sections (60 nm), which were examined under an electron microscope (JEOL JEM-1010, Tokyo, Japan).

MitoTracker and Senescence-Associated β-Galactosidase Staining

Frozen sections (3 μm) were prepared for MitoTracker deep red staining (M22426; Thermo Fisher, USA) according to the manufacturer's instructions to assess mitochondrial mass. Images were captured by confocal microscopy (Leica TCS SP2 AOBS; Leica Microsystems, Buffalo Grove, IL, USA). Frozen sections (3 μm) or cells cultured on coverslips were prepared for senescence-associated β-galactosidase (SA-β-gal) staining (#9860; Cell Signaling Technology) according to the protocols to assess renal senescence. Images were taken by the DP27-CU camera coupled to BX-43F microscope (Olympus, Japan).

Methyl Thiazolyl-Tetrazolium Assay and EdU Staining

To assess the effect of ICG-001 or KYA1797K on cell survival, methyl thiazolyl-tetrazolium (MTT) assay was performed. Cells seeded in 96-well were treated with ICG-001 or KYA1797K at different concentrations for 48 h, then 10 μL MTT (0210222701; Weijia Technology, China) at 5 mg/mL was added into each well. After incubation at 37°C for 6 h, the medium was removed, and 150 μL of dimethyl sulfoxide was added. The absorbance of each well was measured at 490 nm using an enzyme-linked immunosorbent assay reader (Synergy HTX; Biotek, USA), and the value represents the number of alive cells. Cultured cells were also stained for measuring the cell's ability to proliferate via EdU (C10637; Invitrogen, USA) staining according to the manufacturer's instructions. Im-

Fig. 1. Aged kidney is associated with upregulation of β-catenin and mitochondrial dysfunction. **a–c** Representative Western blot and quantitative data showing renal expression of active β-catenin and β-catenin from 2-month-old and 24-month-old mice. Numbers (1–5) indicate each individual animal in a given group. Statistical significance was determined by two-side Student's *t* test. $^{**}p < 0.01$, $^{***}p < 0.001$ versus 2-month-old mice group. **d** Representative micrographs showing active β-catenin (left) and PGC-1α (right) expression in kidneys from 2-month-old and 24-month-old mice. Cryosections were subjected to fluorescence staining for active β-catenin. Paraffin-embedded kidney sections were immunostained with an antibody against PGC-1α. Arrows indicate positive staining. Scale bar, 50 μm. **e–g** Representative Western blot and quantitative data showing renal expression of PGC-1α and TOMM20. Numbers (1–5) indicate each individual animal in a given group. Statistical significance was determined by two-side Student's *t* test. $^{**}p < 0.01$, $^{***}p < 0.001$ versus 2-month-old mice group. **h** Representative fluorescence and TEM micrographs show mitochondrial mass (top) and mitochondrial ultrastructure morphology (bottom). The frozen kidney sections were stained with MitoTracker deep red (3 μm). Ultrathin kidney sections were studied using a transmission electron microscope. For MitoTracker, arrows indicate positive staining; For TEM analyses, arrow indicates abnormal characteristics of swollen shape and fragmented cristae in mitochondria. Scale bar, 50 μm for MitoTracker; 1 μm for electron microscope micrographs. TEM, transmission electron microscopy. **i–o** Representative Western blot and quantitative data showing renal expression of Klotho, P19ARF, γH2AX, P16INK4A, fibronectin, and α-SMA. Numbers (1–5) indicate each individual animal in a given group. Statistical significance was determined by two-side Student's *t* test. $^{***}p < 0.001$ versus 2-month-old mice group.

(For figure see next page.)

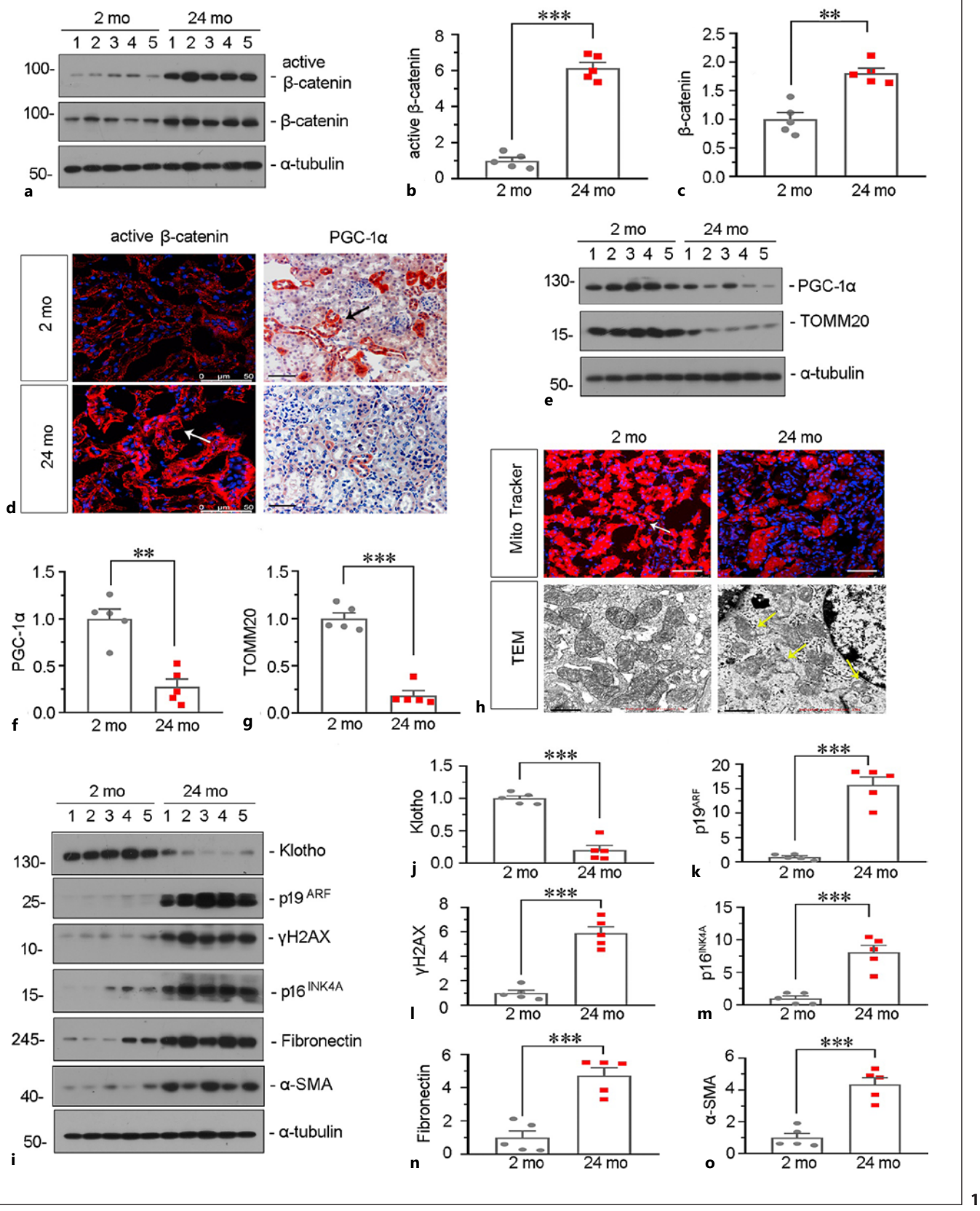
2 mo
24 mo
1 2 3 4 5 1 2 3 4 5
100-
active β-catenin
100-
- β-catenin
50-
- α-tubulin
a
***
active β-catenin
2 mo
24 mo
b
**
β-catenin
2 mo
24 mo
c
active β-catenin
PGC-1α
2 mo
24 mo
d
130-
- PGC-1α
15-
- TOMM20
50-
- α-tubulin
e
**
PGC-1α
2 mo
24 mo
f
***
TOMM20
2 mo
24 mo
g
Mito Tracker
TEM
h
130-
- Klotho
25-
- p19 ARF
10-
- γH2AX
15-
- p16 INK4A
245-
- Fibronectin
40-
- α-SMA
50-
- α-tubulin
i
Klotho
j
p19ARF
k
γH2AX
l
p16INK4A
m
Fibronectin
n
α-SMA
o

1

ages were captured by confocal microscopy (Leica TCS SP2 AOBS; Leica Microsystems).

Immunofluorescence Staining

Immunofluorescence staining was performed to assess the effect of ICG-001 or KYA1797K on active β-catenin, mitochondrial function, renal fibrosis, and renal senescence. Kidney cryosections and HKC-8 cells cultured on coverslips were fixed with 4% paraformaldehyde for 15 min at room temperature, followed by blocking with 10% donkey serum for 1 h. Then the slides were stained with special primary antibodies overnight at 4°C and stained with a Cy3- or Cy2-conjugated secondary antibody (Jackson ImmunoResearch Laboratories, USA) for 1 h at room temperature. Nuclei were stained with DAPI (C1006; Beyotime, China) according to manufacturer's instructions. Images were captured by confocal microscopy (Leica TCS SP2 AOBS; Leica Microsystems). The primary antibodies used were as follows: anti-fibronectin (1:100; F3648, Sigma-Aldrich), anti-γH2AX (1:80; ab26350, Abcam), anti-active β-catenin (1:80; 19807s, Cell Signaling Technology), anti-TOMM20 (1:100; ab186735, Abcam).

Measurements of Serum Creatinine, Serum Urea, and Ualb Levels

Serum creatinine and urea were measured by an automatic chemistry analyzer (AU480 Chemistry Analyzer; Beckman Coulter). Ualb levels and urine creatinine (Ucr) were tested by a mouse Albumin ELISA Quantitation kit (CSB-E13878m, CUSABIO, USA) or creatinine ELISA Quantitation kit (DICT-500; BioAssay Systems, USA) according to the manufacturer's protocol. Ualb was normalized to Ucr and expressed as microgram per milligram Ucr.

Statistical Analyses

The data were expressed as the mean ± standard error of the mean. SPSS 20.0 (SPSS Inc, Chicago, IL, USA) was used for statistical analysis. Before comparison, all data were firstly analyzed for normal distribution using the D'Agostino normality test. Student's *t* test was used to determine differences between groups. p value < 0.05 was considered to be statistically significant.

Results

Aged Kidney Is Associated with Upregulation of β-Catenin and Mitochondrial Dysfunction

To identify the role of β-catenin in aging, the expression of β-catenin in naturally aging mice was assessed. Compared with 2-month-old mice, the expression levels of active β-catenin and β-catenin were upregulated in 24-month-old mice (Fig. 1a–c). Similar result was demonstrated by immunofluorescence staining of active β-catenin (Fig. 1d).

On the other hand, the mitochondrial function was impaired in aged kidneys. Immunohistochemical staining showed that the expression of peroxisome proliferator-activated receptor-C coactivator-1α (PGC-1α) was downregulated in aged mice (Fig. 1d). Besides, Western blot analysis of PGC-1α and translocase of outer mitochondrial membrane 20 (TOMM20) also indicated similar results (Fig. 1e–g). Furthermore, the mitochondrial mass examined by MitoTracker staining was significantly lower, and the mitochondrial morphology tested by TEM was obviously impaired in 24-month-old mice (Fig. 1h).

We then assessed renal senescence in aged kidney. As shown in Figure 1i–m, the expressions of $P16^{INK4A}$, γH2AX, and $P19^{ARF}$ were greatly increased in 24-month-old mice, while the expression of Klotho, an antiaging protein, was downregulated. In addition, renal fibrosis in aged kidneys was also assessed, and the results showed that the expressions of fibronectin, α-smooth muscle actin (α-SMA) were greatly increased in 24-month-old mice (Fig. 1i, n, and o).

KYA1797K Is Superior to ICG-001 to Inhibit β-Catenin Signaling in the Accelerated Aging Mouse Model

To further investigate the effects of β-catenin and its inhibitor, we established an accelerated aging model of mouse (Fig. 2a). In this model, the expressions of active β-catenin and β-catenin were upregulated by D-gal but were obviously inhibited by ICG-001 or KYA1797K treatment (Fig. 2b–d). However, the inhibitory effects of KYA1797K were more significant than ICG-001. Similar result was demonstrated when the expression of active-β-catenin was assessed by immunofluorescence staining (Fig. 2e). We also examined the expression of serum creatinine, serum urea, and Ualb in different groups, but there was no statistical difference (Fig. 2f–h).

KYA1797K Is Superior to ICG-001 to Alleviate Renal Fibrosis in Kidneys in the Accelerated Aging Mouse Model

We then tested renal fibrosis in the accelerated aging mice model. Western blot analyses showed that the expressions of fibronectin and α-SMA were upregulated by D-gal treatment, while the expression of Klotho was downregulated (Fig. 3a–d). However, ICG-001 or KYA1797K treatment reversed their expressions. Compared with ICG-001, KYA1797K had a stronger effect. Similar result was demonstrated by the immunohistochemical staining of fibronectin and Sirius red staining of fibrotic lesions (Fig. 3e). These results further confirmed the protective role of ICG-001 and KYA1797K in age-related kidney fibrosis, in which the latter had a better effect.

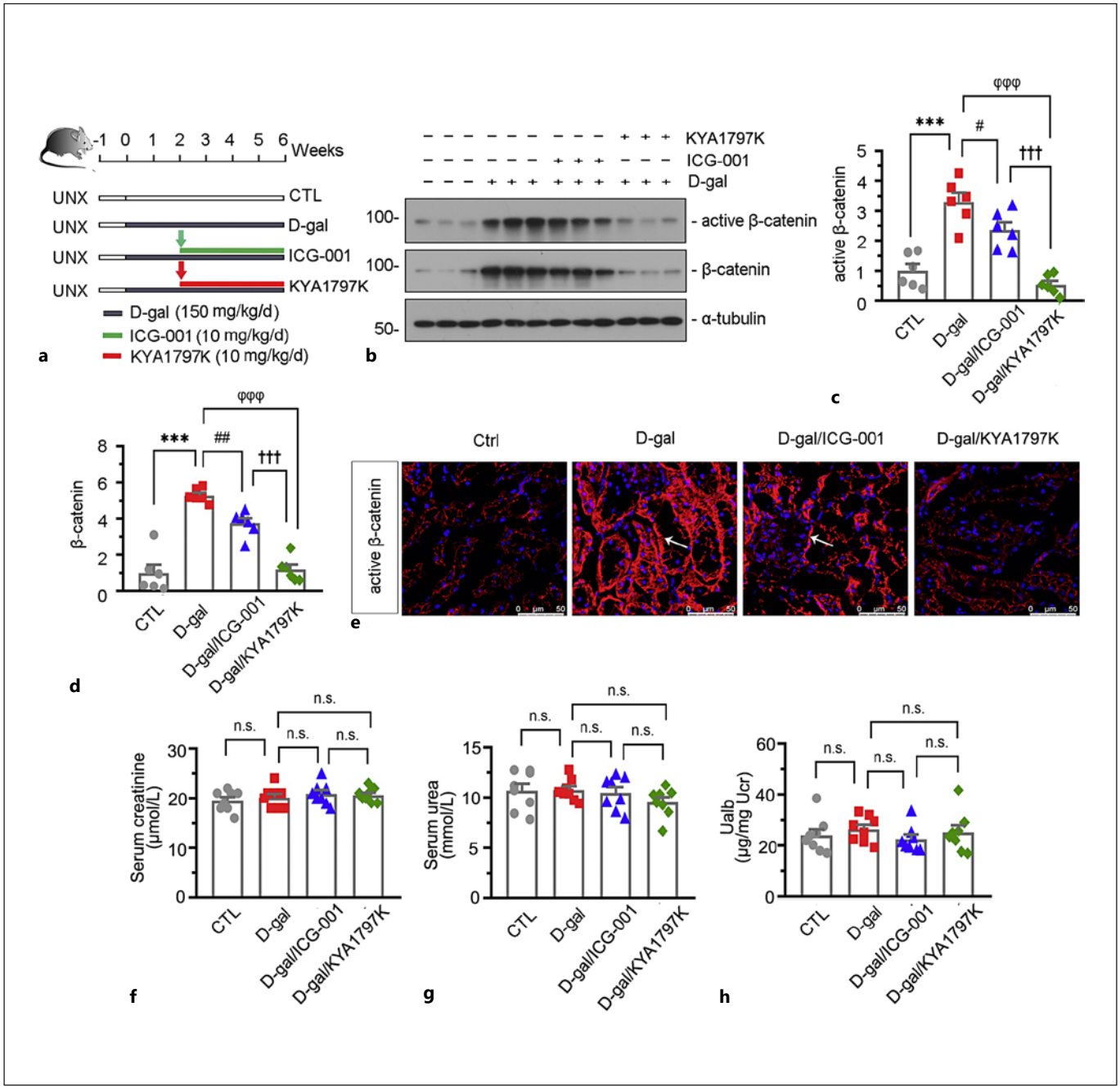

Fig. 2. KYA1797K is superior to ICG-001 to inhibit β-catenin signaling in the accelerated aging mouse model. **a** Experimental design. Black bar-indicated mice were administered subcutaneous injections of D-gal at 150 mg/kg/day for 6 weeks after UNX surgery for 1 week. Green bar- and red bar-indicated mice were administered intraperitoneal injections of ICG-001 at 10 mg/kg/day or KYA1797K at 10 mg/kg/day for 4 weeks after 2 weeks' injection of D-gal. UNX: unilateral nephrectomy. **b–d** Representative Western blot and quantitative data showing renal expression of active β-catenin and β-catenin. Statistical significance was determined by two-side Student's *t* test. $^{***}p < 0.001$ versus control mice group alone; $^{\#}p < 0.05$, $^{\#\#}p < 0.01$ versus the D-gal-treated mice group alone; $^{\dagger\dagger\dagger}p < 0.001$ versus D-gal + ICG-001 group alone; $^{\varphi\varphi\varphi}p < 0.001$ versus the D-gal-treated mice group alone ($n = 6$). **e** Representative micrographs showing renal expression of active β-catenin in different groups. Cryosections were immunostained with an antibody against active β-catenin. Arrows indicate positive staining. Scale bar, 50 μm. **f–h** Graphical representation of the levels of serum creatinine, serum urea, and Ualb in different groups. Urinary albumin (Ualb) was normalized to urinary creatinine (Ucr) and expressed as microgram per milligram Ucr. Statistical significance was determined by two-side Student's *t* test. n.s., none of significance ($n = 8$).

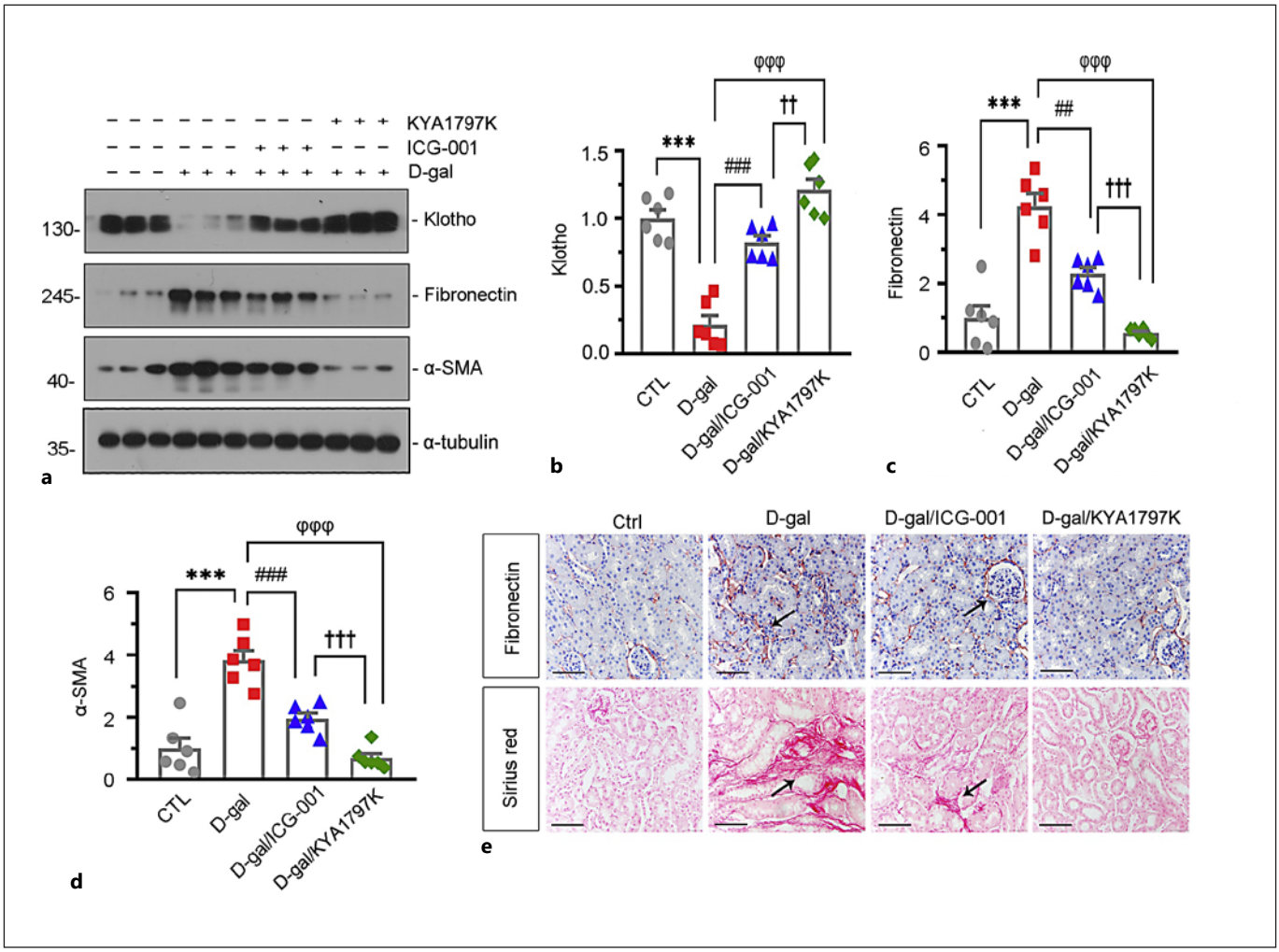

Fig. 3. KYA1797K is superior to ICG-001 to alleviate renal fibrosis in kidneys in the accelerated aging mouse model. **a–d** Representative Western blot and quantitative data showing renal expression of Klotho, fibronectin, and α-SMA. Statistical significance was determined by two-side Student's *t* test. $^{***}p < 0.001$ versus the control mice group alone; $^{\#\#}p < 0.01$, $^{\#\#\#}p < 0.001$ versus the D-gal-treated mice group alone; $^{\dagger\dagger}p < 0.01$, $^{\dagger\dagger\dagger}p < 0.001$ versus D-gal + ICG-001 group alone; $^{\varphi\varphi\varphi}p < 0.001$ versus the D-gal-treated mice group alone ($n = 6$). **e** Representative micrographs showing Sirius red staining and renal expression of fibronectin in different groups. Paraffin-embedded kidney sections were immunostained with Sirius red and an antibody against fibronectin. Arrows indicate positive staining. Scale bar, 50 μm.

KYA1797K Is Superior to ICG-001 to Protect against Cell Senescence in Kidneys in the Accelerated Aging Mouse Model

We next examined cellular senescence. Western blot analysis showed that the upregulation of $P16^{INK4A}$, γH2AX, and $P19^{ARF}$ induced by D-gal was downregulated by ICG-001 or KYA1797K (Fig. 4a–d). Similarly, KYA1797K has a stronger inhibitory effect. Besides, the SA-β-gal staining of β-galactosidase activity and immunohistochemical staining of $P16^{INK4A}$ also showed similar results (Fig. 4e). These results suggest that β-catenin inhibitor could alleviate renal senescence, and the protective effect of KYA1797K is superior to that of ICG-001.

KYA1797K Is Superior to ICG-001 to Maintain Mitochondrial Homeostasis in Kidneys in the Accelerated Aging Mouse Model

We next investigated the protective effects of β-catenin inhibitor on mitochondrial dysfunction. Western blot analysis showed that D-gal induced downregulation of PGC-1α and TOMM20, but ICG-001 or

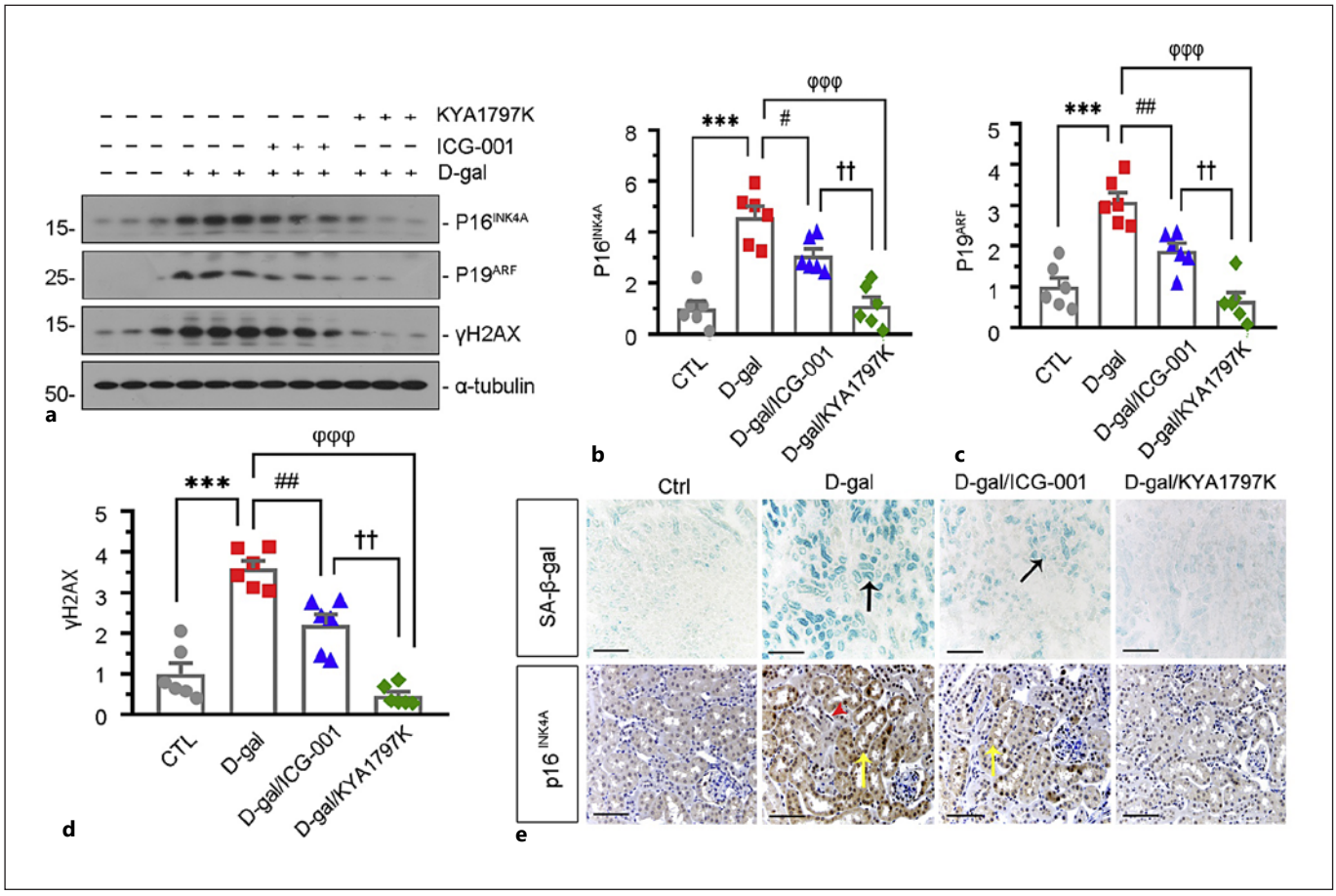

Fig. 4. KYA1797K is superior to ICG-001 to protect against cell senescence in kidneys in the accelerated aging mouse model. **a–d** Representative Western blot and quantitative data showing renal expression of $p16^{INK4A}$, $p19^{ARF}$, and γH2AX. Statistical significance was determined by two-side Student's *t* test. $^{***}p < 0.001$ versus the control mice group alone; $^{\#}p < 0.05$, $^{\#\#}p < 0.01$ versus the D-gal-treated mice group alone; $^{\dagger\dagger}p < 0.01$ versus D-gal + ICG-001 mice group alone; $^{\varphi\varphi\varphi}p < 0.001$ versus the D-gal-treated mice group alone ($n = 6$). **e** Representative micrographs showing senescence via β-galactosidase activity (SA-β-gal) and renal expression of $p16^{INK4A}$ in different groups. Frozen kidney sections were stained for SA-β-gal (top). Black arrows indicate positive staining. Paraffin-embedded kidney sections were immunostained with an antibody against $p16^{INK4A}$ (bottom). Yellow arrows indicate positive staining of renal tubules. Red arrowhead indicates positive staining of renal interstitial cell. Scale bar, 50 μm.

Fig. 5. KYA1797K is superior to ICG-001 to maintain mitochondrial homeostasis in kidneys in the accelerated aging mouse model. **a–c** Representative Western blot and quantitative data showing renal expression of PGC-1α and TOMM20. Statistical significance was determined by two-side Student's *t* test. $^{**}p < 0.01$, $^{***}p < 0.001$ versus control mice group alone; $^{\#\#\#}p < 0.001$ versus the D-gal-treated mice group alone; $^{\dagger\dagger\dagger}p < 0.001$ versus D-gal + ICG-001 group alone; $^{\varphi\varphi\varphi}p < 0.001$ versus the D-gal-treated mice group alone ($n = 6$). **d** Representative micrographs showing mitochondrial mass, mitochondrial ultrastructure morphology, and renal expression of PGC-1α and TOMM20 in different groups. Paraffin-embedded kidney sections were immunostained with an antibody against PGC-1α. The frozen kidney sections were stained with MitoTracker deep red (3 μm) and TOMM20. Ultrathin kidney sections were studied using a transmission electron microscope. For MitoTracker, PGC-1α, and TOMM20, arrows indicate positive staining; For TEM analyses, arrow indicates abnormal characteristics of swollen shape and fragmented cristae in mitochondria. Scale bar, 50 μm for staining of PGC-1α, TOMM20, and MitoTracker; 1 μm for electron microscope micrographs. TEM, transmission electron microscopy. **e** Graphical representation of the number of abnormal mitochondria in different groups. The average number of abnormal mitochondria of five renal tubular epithelial cells per mouse were analyzed for quantification in different groups. Statistical significance was determined by two-side Student's *t* test. $^{***}p < 0.001$ versus the control mice group alone; $^{\#\#\#}p < 0.001$ versus the D-gal-treated mice group alone; $^{\dagger\dagger\dagger}p < 0.001$ versus D-gal + ICG-001 mice group alone; $^{\varphi\varphi\varphi}p < 0.001$ versus the D-gal-treated mice group alone ($n = 5$).

(For figure see next page.)

KYA1797K restored their expressions (Fig. 5a–c). Similar result was demonstrated by immunohistochemical analysis for PGC-1α and immunofluorescence staining for TOMM20 (Fig. 5d). Besides, the results of Mito-Tracker staining and TEM showed that the mitochondrial mass loss (Fig. 5d) and impairment of mitochondrial morphology (Fig. 5d, e) induced by D-gal were also inhibited by ICG-001 or KYA1797K treatment. Similarly, the protective effects of KYA1797K were more significant than ICG-001.

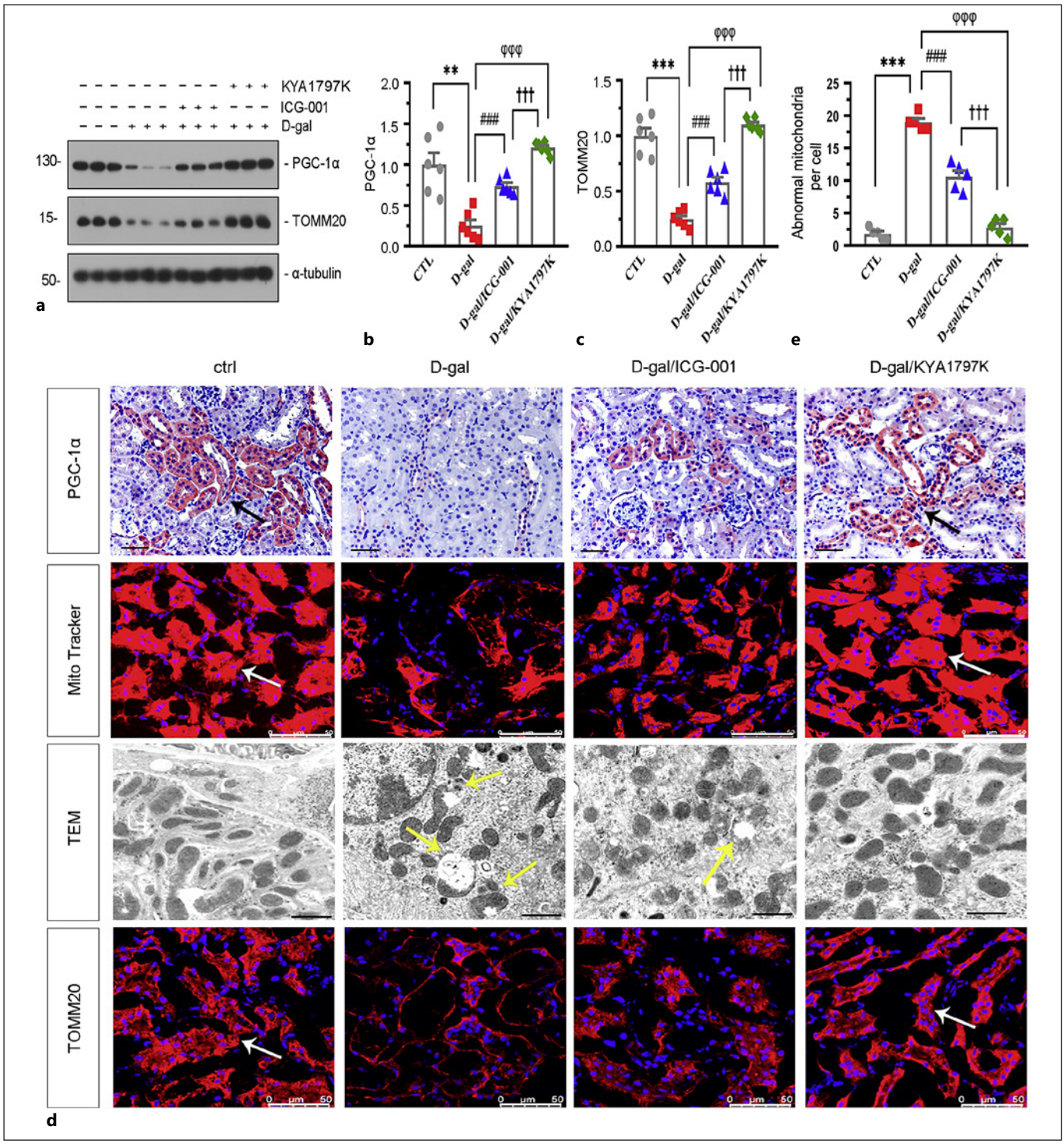

5

Kidney Dis 2022;8:408–423
DOI: 10.1159/000526139

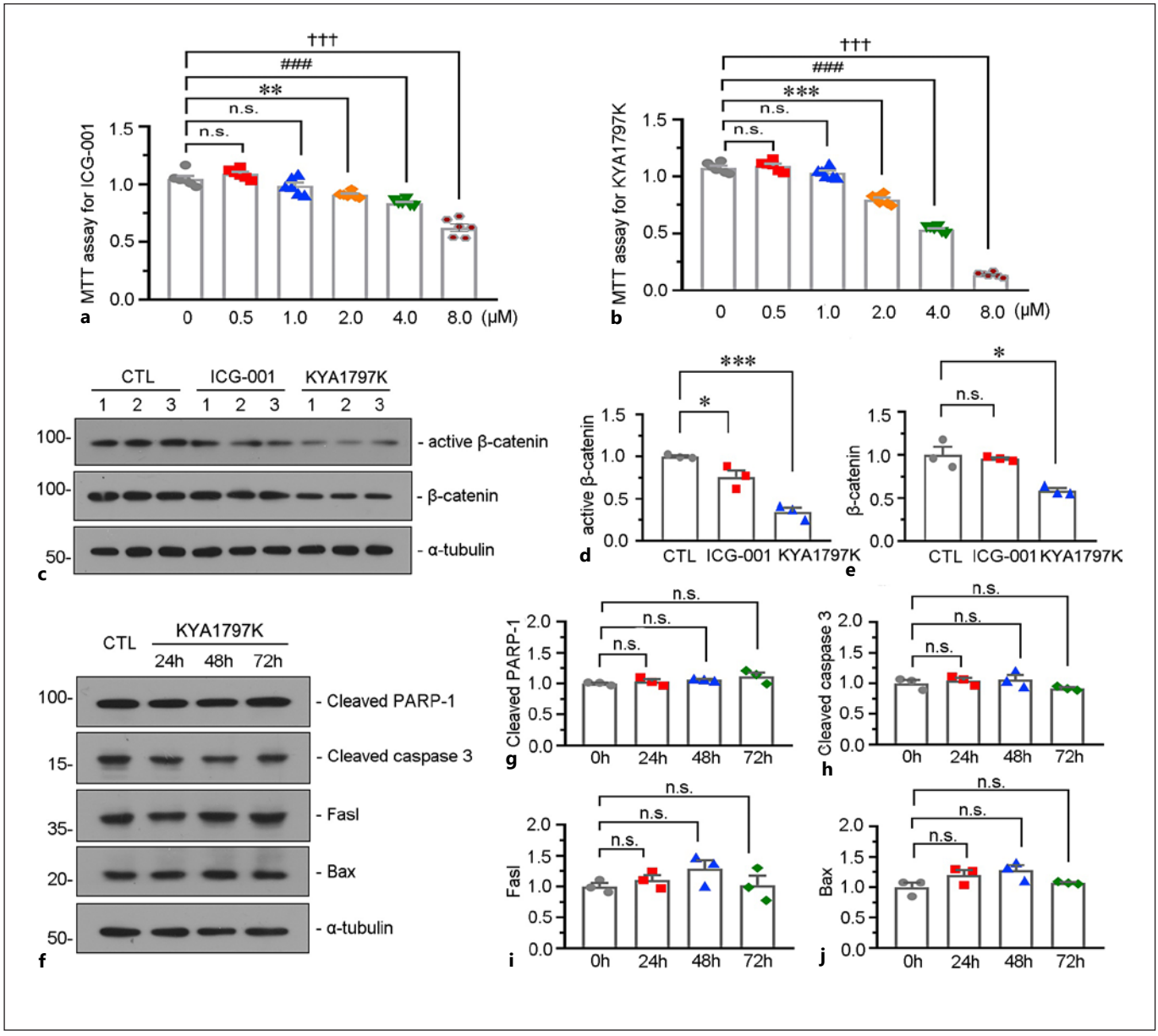

Fig. 6. KYA1797K is superior to ICG-001 to inhibit β-catenin signaling in vitro and shows no apoptosis-inducing effects at the indicated concentration. **a**, **b** Quantitative data showing MTT assay of ICG-001 and KYA1797K in HKC-8 cells. The y-axis represented OD value in each group. HKC-8 cells were treated with ICG-001 (**a**) or KYA1797K (**b**) at 0 μM, 0.5 μM, 1.0 μM, 2.0 μM, 4.0 μM, and 8.0 μM for 48 h, respectively. Statistical significance was determined by two-side Student's *t* test. ns versus 0 μM group; $^{**}p < 0.01$, $^{***}p < 0.001$, $^{\#\#\#}p < 0.001$, $^{\dagger\dagger\dagger}p < 0.001$ versus 0 μM group ($n = 6$). ns, none of significance. **c–e** Representative Western blot and quantitative data showing the expression of active β-catenin and β-catenin in HKC-8 cells. HKC-8 cells were treated with ICG-001 or KYA1797K at 1 μM for 60 h. Statistical significance was determined by two-side Student's *t* test. ns versus control group alone; $^{*}p < 0.05$, $^{***}p < 0.001$ versus control group alone ($n = 3$). ns, none of significance. **f–j** Representative Western blot and quantitative data showing the expression of cleaved PARP-1, cleaved caspase-3, Fasl, and BAX in HKC-8 cells. HKC-8 cells were treated with KYA1797K (1 μM) for 24 h, 48 h, and 72 h, respectively. Statistical significance was determined by two-side Student's *t* test. ns versus control group alone ($n = 3$). ns, none of significance.

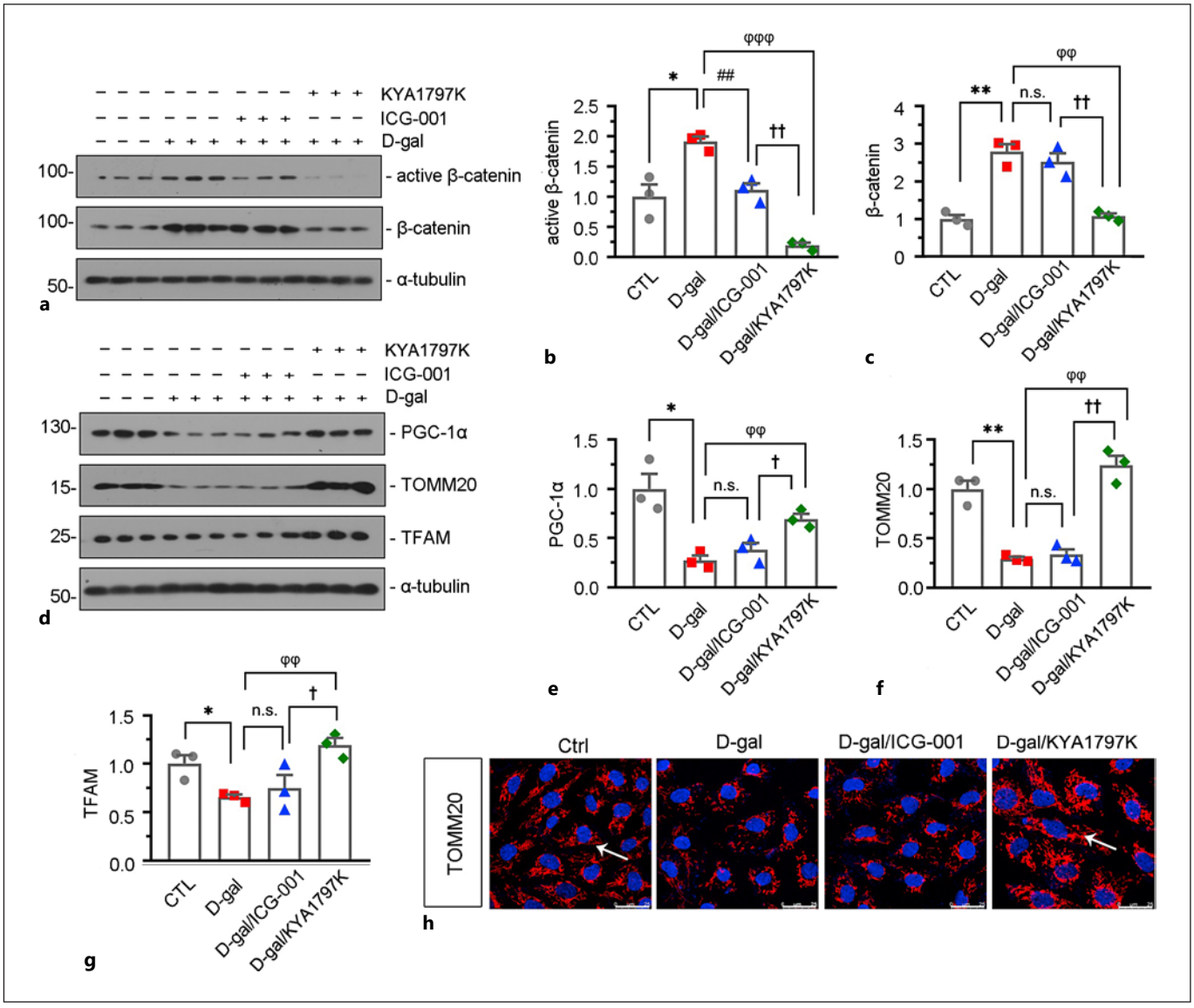

Fig. 7. KYA1797K is far better than ICG-001 to protect mitochondrial function in vitro. **a–g** Representative Western blot (**a**, **d**) and quantitative data (**b**, **c**, **e–g**) showing the expression of active β-catenin, β-catenin, PGC-1α, TOMM20, and TFAM in HKC-8 cells. HKC-8 cells were pretreated with ICG-001 and KYA1797K at 1 μM for 1 h, followed by treatment with D-gal at 10 mg/mL for 60 h. Statistical significance was determined by two-side Student's *t* test. $^{*}p < 0.05$, $^{**}p < 0.01$ versus the control group alone; ns versus D-gal-treated group alone, $^{\#\#}p < 0.01$ versus the D-gal-treated group alone; $^{\dagger}p < 0.05$, $^{\dagger\dagger}p < 0.01$ versus D-gal + ICG-001 group alone; $^{\varphi\varphi}p < 0.01$, $^{\varphi\varphi\varphi}p < 0.001$ versus the D-gal-treated group alone ($n = 3$). ns, none of significance. **h** Representative micrographs showing the expression of TOMM20 in different groups. HKC-8 cells cultured on coverslips were immunostained with an antibody against TOMM20. Arrows indicate positive staining. Scale bar, 25 μm.

KYA1797K Is Superior to ICG-001 to Inhibit β-Catenin Signaling in vitro and Shows No Apoptosis-Inducing Effects at the Indicated Concentration

We then investigated the role of ICG-001 and KYA1797K in cellular aging in vitro. HKC-8 cell is an optimized differentiated human renal epithelial cell line and is commonly used for the study of renal injury or disease [35]. First, MTT assay was performed, and results showed that it was safe to treat the cells with ICG-001 or KYA1797K at the concentration of 1 μM (Fig. 6a, b), which concentration was used in the subsequent experiments. Then HKC-8 cells were treated with ICG-001 or KYA1797K for 60 h

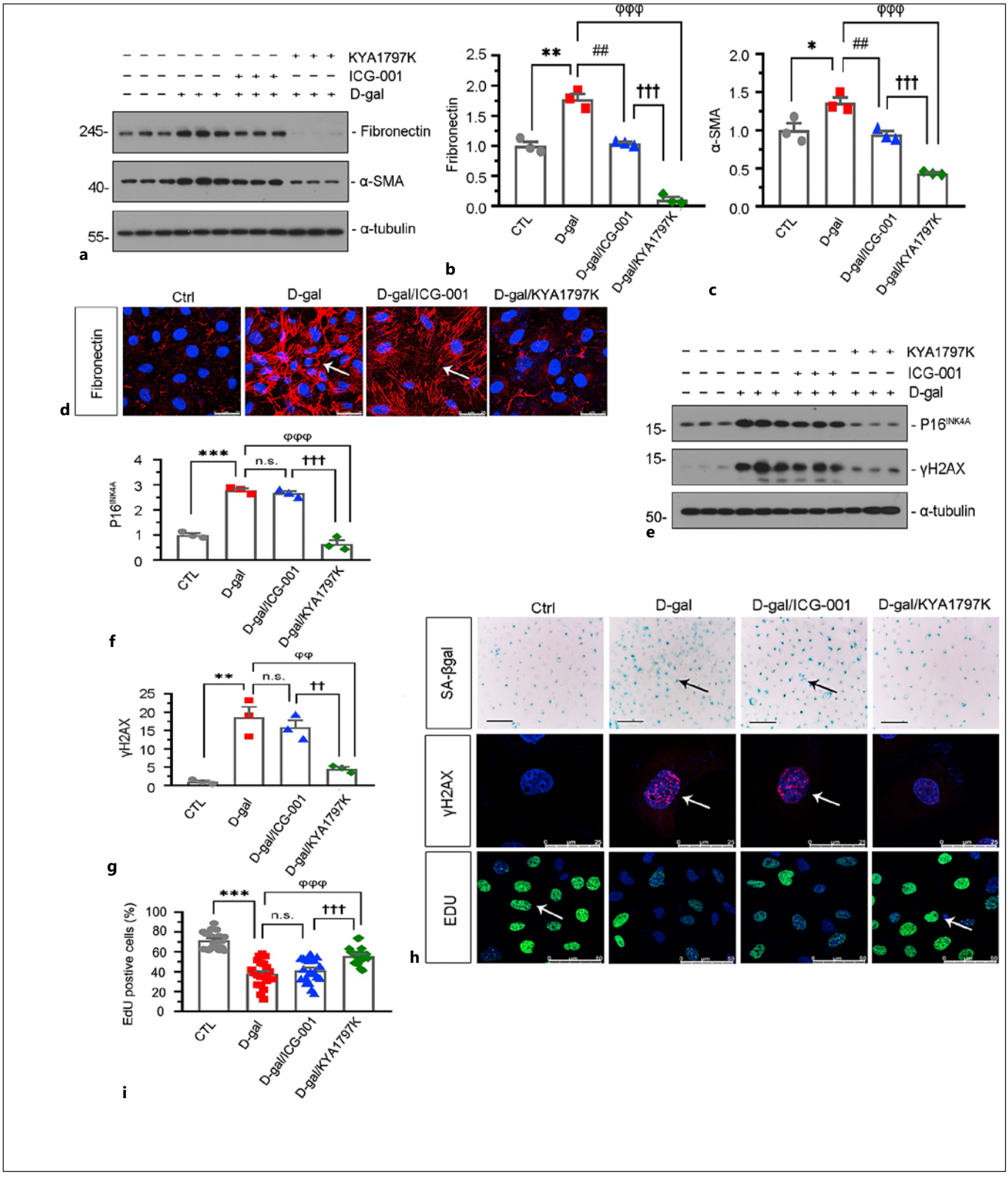

8

(For legend see next page.)

to compare their inhibitory effects on β-catenin. Western blot showed that both ICG-001 and KYA1797K downregulated the expressions of active β-catenin (Fig. 6c–e). However, ICG-001 could not inhibit the expression of total β-catenin, while KYA1797K still had inhibitory effect. Since the cells would be treated for 60 h, the influence of KYA1797K on cellular apoptosis was detected. The expression of cleaved PARP-1, cleaved caspase-3, Fasl, and BAX had no difference over 72 h (Fig. 6f–j).

KYA1797K Is Far Better than ICG-001 to Protect Mitochondrial Function in vitro

We next examined the effects of ICG-001 and KYA1797K on β-catenin and mitochondrial functions in vitro. Western blot showed that the expressions of active β-catenin and β-catenin were upregulated by D-gal, and KYA1797K could restore both of their expressions, while ICG-001 only inhibited the expression of active β-catenin (Fig. 7a–c). Besides, the inhibitory effect of KYA1797K on active β-catenin was more significant than that of ICG-001. We then assessed their protective effects on mitochondrial functions. The expressions of PGC-1α, TOMM20, and mitochondrial transcription factor A (TFAM) were downregulated by D-gal, but only KYA1797K restored their expressions (Fig. 7d–g). Similar result was also observed by analysis of immunofluorescence staining for TOMM20 (Fig. 7h).

KYA1797K Is Superior to ICG-001 to Retard Cellular Senescence and Age-Related Fibrotic Lesions in vitro

The cellular fibrosis and senescence were also examined in vitro. The upregulation of fibronectin and α-SMA induced by D-gal was inhibited by ICG-001 or KYA1797K treatment (Fig. 8a–c). Compared with ICG-001, KYA1797K still had a stronger effect. Besides, immunofluorescence staining of fibronectin also showed a similar result (Fig. 8d). We then assessed their effects on cellular senescence. The upregulation of $P16^{INK4A}$ and γH2AX induced by D-gal showed no change after ICG-001 treatment but was inhibited by KYA1797K treatment (Fig. 8e–g). Similar result was shown by immunofluorescence staining of γH2AX and SA-β-gal staining for β-galactosidase activity (Fig. 8h). In addition, the effects of ICG-001 and KYA1797K on the proliferative ability of cells were assessed by EdU staining. The inhibition of the proliferative activity of HKC-8 cells induced by D-gal was restored by KYA1797K, while ICG-001 treatment showed no effect (Fig. 8h–i).

Discussion

Aging has become a serious social problem for the whole world [36]. Notably, up to 2050, the elderly people would make up to 20% of the whole population [37]. Aging is a key risk factor for the function disturbance in organs [38, 39]. As one of the most important organs in the body, the kidney exerts the function of excretion, reabsorption, filtration, and endocrine modulation [3, 40]. Aging acts as a critical mediator in the high morbidity of kidney injury and accelerated renal dysfunction [4, 41]. However, the underlying mechanisms of kidney aging are still in mystery. Our previous study has shown that the activation of Wnt/β-catenin signaling plays an important role in the acceleration of renal tubular cell senescence

Fig. 8. KYA1797K is superior to ICG-001 to retard cellular senescence and age-related fibrotic lesions in vitro. **a–c** Representative Western blot and quantitative data showing the expression of fibronectin and α-SMA in HKC-8 cells. HKC-8 cells were pretreated with ICG-001 and KYA1797K at 1 μM for 1 h, followed by treatment with D-gal at 10 mg/mL for 60 h. Statistical significance was determined by two-side Student's *t* test. $^{*}p < 0.05$, $^{**}p < 0.01$ versus the control group alone; $^{\#\#}p < 0.01$ versus the D-gal-treated group alone; $^{\dagger\dagger\dagger}p < 0.001$ versus D-gal + ICG-001 group alone; $^{\varphi\varphi\varphi}p < 0.001$ versus the D-gal-treated group alone ($n = 3$). **d** Representative micrographs showing the expression of fibronectin in different groups. HKC-8 cells cultured on coverslips were immunostained with an antibody against fibronectin. Arrows indicate positive staining. Scale bar, 25 μm. **e–g** Representative Western blot and quantitative data showing the expression of $p16^{INK4A}$ and γH2AX in HKC-8 cells. Statistical significance was determined by two-side Student's *t* test. $^{**}p < 0.01$, $^{***}p < 0.001$ versus the control group alone; ns versus the D-gal-treated group alone; $^{\dagger\dagger}p < 0.01$, $^{\dagger\dagger\dagger}p < 0.001$ versus D-gal + ICG-001 group alone; $^{\varphi\varphi}p < 0.01$, $^{\varphi\varphi\varphi}p < 0.001$ versus the D-gal-treated group alone ($n = 3$). ns: none of significance. **h** Representative micrographs showing senescence via β-galactosidase activity (SA-β-gal) and the expression of γH2AX and EdU in different groups. The cells cultured on coverslips were stained for SA-β-gal or immunostained with an antibody against γH2AX and EdU. Arrows indicate positive staining. Scale bar, 25 μm for γH2AX; Scale bar, 50 μm for SA-β-gal and EdU. **i** Graphical representation of the percentage of EdU positive cells in different groups. HKC-8 cells cultured on the coverslips were stained with EdU in different groups, and images were captured from 21 areas (×40) in each group. The percentage of EdU positive cells of each image was analyzed for quantification. Statistical significance was determined by two-side Student's *t* test. $^{***}p < 0.001$ versus the control group alone; ns versus the D-gal-treated group alone; $^{\dagger\dagger\dagger}p < 0.001$ versus D-gal + ICG-001 group alone; $^{\varphi\varphi\varphi}p < 0.001$ versus the D-gal-treated group alone ($n = 21$). ns, none of significance.

and fast-going aging in kidneys [13, 14]. We found β-catenin could not only initiate cellular senescence but also induce mitochondrial dysfunction through inhibition of PGC-1α [13], the key transcription factor which modulates mitochondrial biogenesis. Hence, β-catenin has multifunctional effects on kidney aging process.

Several lines of evidence have shown that β-catenin signaling pathway is associated with multiple organ fibrosis. For example, studies showed that the Wnt/β-catenin signaling pathway was involved in myocardial remodeling in the settings of chronic kidney disease [42] and was required for deposition of fibrotic extracellular matrix and the regulation of cardiomyocyte hypertrophy in a mouse model of heart fibrosis [43]. In the liver, Wnt/β-catenin signaling had been implicated in the pathogenesis of liver fibrosis, and its inhibitor possessed antifibrotic effect [44, 45]. What is more, the studies of pulmonary fibrosis showed that Wnt/β-catenin signaling might be an essential mechanism underlying the regulation of myofibroblast differentiation of lung resident mesenchymal stem cells [46], while the inhibitor of β-catenin was a potent antifibrotic agent for pulmonary fibrosis [47]. All these results suggest that Wnt/β-catenin signaling pathway is one of the therapeutic targets for fibrotic diseases.

Upon the binding of canonical Wnt(s), β-catenin could trigger the transcription of downstream targets through CBP-coactivated TCF/LEF-1 transcription factors [33]. Notably, β-catenin could also bind to FOXO transcription factors such as FOXO4, FOXO1 [29, 48], which are the causal factors in organ aging [49]. FOXO4 is recently reported as a pivot in aging [50], while FOXO6 has also been found increased in aged liver [51] and has a repressive effect in PGC-1α mRNA transcription [52]. These suggest that β-catenin could promote organ aging through multiple pathways. To testify the hypothesis, we compared the therapeutic effects of ICG-001 and KYA1797K in D-gal-induced accelerated aging mice model. As ICG-001 inhibits β-catenin pathway mainly through blocking the binding of β-catenin/TCF/LEF-1 pathway [48], while KYA179K induces the destruction of β-catenin [34], we hypothesized that KYA1797K would be superior to ICG-001 in protecting against kidney aging, since TCF/LEF-1 transcription factors would possibly not be the only downstream effectors.

Several lines of evidence have supported our hypothesis. The correlations of β-catenin and mitochondrial dysfunction and kidney aging were first testified in naturally aging mice (Fig. 1). Notably, in old mice, β-catenin activation is accompanied by loss of PGC-1α and disordered mitochondrial homeostasis, suggesting the regulation of β-catenin in PGC-1α pathway. We next compared the therapeutic effects of KAY1797K and ICG-001. Although ICG-001 could also exhibit some therapeutic effects on fibrosis and senescence in D-gal-treated mice, the efficacy is far less than that of KYA1797K (Fig. 2, 3, 4). We also found that KYA1797K has much more superiority in maintaining mitochondrial homeostasis (Fig. 5). The better efficacy was also proved in vitro. In cultured proximal tubular cells, KYA1797K shows a tremendous therapeutic effect on cellular senescence, mitochondrial disturbance, and fibrotic lesions, at the same dose as that in ICG-001, while ICG-001 could only partly ameliorate fibrotic lesions (Fig. 6–8). These results show that effectively destroying β-catenin is a requisite for retarding kidney aging, since β-catenin could promote other downstream transcription factors besides TCF/LEF-1.

Our results provide an important clue that β-catenin has multifunctional effects on kidney aging process. For example, β-catenin could trigger the upregulation of fibronectin, α-SMA, Snail, PAI-1, and other fibrogenesis-related gene targets through the activation of TCF/LEF-1 transcription factors [26]. Besides, the activation of Wnt/β-catenin leads to mitochondrial dysfunction [13], which would in turn promote further activation of Wnt/β-catenin signaling due to the accumulation of oxidation products [53], thus creating a reciprocal activation loop. Mitochondrial dysfunction causes disease state, which affects the secretion of a variety of cytokines or proteins. β-Catenin inhibitor KYA1797K could alleviate mitochondrial dysfunction and disrupt the vicious cycle, resulting in the improvement of disease state. As a result, the expression of Klotho would also be restored. Interestingly, we recently found that RAS system, the critical player in the pathogenesis of kidney injury [54], and aging [13], is also the downstream target of β-catenin/TCF/LEF-1 pathway [22]. Besides, we also could not exclude the other downstream transcription factors such as FOXOs, would possibly be flared up by β-catenin. Although we could not prove that in the present study, our results at least show that TCF/LEF-1 pathway is not the only downstream effector, since ICG-001 did not exhibit the same efficacy as KYA1797K. Since Wnt/β-catenin signaling has been involved in the pathogenesis of a variety of tissue fibrosis [42–47], we believe that KYA1797K, which could induce the destabilization of β-catenin, may also have beneficial effects on these fibrotic disorders.

There are also some limitations to our study. First of all, the experimental design is relatively simple. Only one animal model is established, and the results need to be further validated in natural aging mice. What is more, we do

not examine other transcription factors associated with aging, such as the FOXOs family which may also be the downstream effector of β-catenin. Although more studies are needed, our study shows that effectively eliminating β-catenin is a more ideal strategy to target kidney aging.

Statement of Ethics

The animal studies were approved by the Experimental Animal Ethics Committee at the Nanfang Hospital, Southern Medical University. The immortalized cell line used in this study were purchased from Dr. L. Racusen (Johns Hopkins University, Baltimore, MD, USA). Ethical approval for the use of these cells is not required in accordance with local/national guidelines.

Conflict of Interest Statement

The authors have no conflicts of interest to declare.

Funding Sources

This work was supported by National Key R&D Program of China (2020YFC2005000), National Natural Science Foundation of China Grant 82225010, 82070707, 91949114; and the project of Innovation team of chronic kidney disease with integrated traditional Chinese and Western Medicine (2019KCXTD014); and Outstanding Youths Development Scheme of Nanfang Hospital, Southern Medical University (2019J013, 2021J001) and the Presidential Foundation of Nanfang Hospital (Grant No. 2019Z006), and Guangdong Provincial Clinical Research Center for Kidney Disease (No. 2020B1111170013).

Author Contributions

Lili Zhou, Maosheng Wang, and Yaozhong Kong conceived the research; Mingsheng Zhu and Lili Zhou designed the experiments and wrote the manuscript; Mingsheng Zhu, Xian Ling, Shan Zhou, Ping Meng, Qiyan Chen, Shuangqin Chen, Kunyu Shen, and Chao Xie performed the experiments; Mingsheng Zhu, Xian Ling, Shan Zhou, and Lili Zhou analyzed the data; Mingsheng Zhu, Xian Ling, and Lili Zhou created the figures. All authors approved the final version of the manuscript.

Data Availability Statement

All data generated or analyzed during this study are included in this article. Further inquiries can be directed to the corresponding author.

References

1 Zhou C, He Q, Gan H, Zeng T, Liu Q, Moorhead JF, et al. Hyperphosphatemia in chronic kidney disease exacerbates atherosclerosis via a mannosidases-mediated complex-type conversion of SCAP N-glycans. Kidney Int. 2021;99(6):1342–53.
2 Isaka Y, Hamano T, Fujii H, Tsujimoto Y, Koiwa F, Sakaguchi Y, et al. Optimal phosphate control related to coronary artery calcification in dialysis patients. J Am Soc Nephrol. 2021;32(3):723–35.
3 Scholz H, Boivin FJ, Schmidt-Ott KM, Bachmann S, Eckardt KU, Scholl UI, et al. Kidney physiology and susceptibility to acute kidney injury: implications for renoprotection. Nat Rev Nephrol. 2021;17(5):335–49.
4 Inker LA, Okparavero A, Tighiouart H, Aspelund T, Andresdottir MB, Eiriksdottir G, et al. Midlife blood pressure and late-life GFR and albuminuria: an elderly general population cohort. Am J Kidney Dis. 2015;66(2):240–8.
5 Salminen A. Feed-forward regulation between cellular senescence and immunosuppression promotes the aging process and age-related diseases. Ageing Res Rev. 2021;67:101280.
6 Xiong Y, Zhou L. The signaling of cellular senescence in diabetic nephropathy. Oxid Med Cell Longev. 2019;2019:7495629.
7 Hagen M, Derudder E. Inflammation and the alteration of B-cell physiology in aging. Gerontology. 2020;66(2):105–13.
8 Kioussis B, Tuttle CSL, Heard DS, Kennedy BK, Lautenschlager NT, Maier AB. Targeting impaired nutrient sensing with repurposed therapeutics to prevent or treat age-related cognitive decline and dementia: a systematic review. Ageing Res Rev. 2021;67:101302.
9 Zhou L, Li Y, Zhou D, Tan RJ, Liu Y. Loss of klotho contributes to kidney injury by derepression of Wnt/β-catenin signaling. J Am Soc Nephrol. 2013;24(5):771–85.
10 Kawai M, Kinoshita S, Ozono K, Michigami T. Inorganic phosphate activates the AKT/mTORC1 pathway and shortens the life span of an α-Klotho-deficient model. J Am Soc Nephrol. 2016;27(9):2810–24.
11 Zhou X, Chen K, Lei H, Sun Z. Klotho gene deficiency causes salt-sensitive hypertension via monocyte chemotactic protein-1/CC chemokine receptor 2-mediated inflammation. J Am Soc Nephrol. 2015;26(1):121–32.
12 Zhu L, Stein LR, Kim D, Ho K, Yu GQ, Zhan L, et al. Klotho controls the brain-immune system interface in the choroid plexus. Proc Natl Acad Sci U S A. 2018;115(48):E11388–96.
13 Miao J, Liu J, Niu J, Zhang Y, Shen W, Luo C, et al. Wnt/β-catenin/RAS signaling mediates age-related renal fibrosis and is associated with mitochondrial dysfunction. Aging Cell. 2019;18(5):e13004.
14 Luo C, Zhou S, Zhou Z, Liu Y, Yang L, Liu J, et al. Wnt9a promotes renal fibrosis by accelerating cellular senescence in tubular epithelial cells. J Am Soc Nephrol. 2018;29(4):1238–56.
15 Hernandez-Segura A, Nehme J, Demaria M. Hallmarks of cellular senescence. Trends Cell Biol. 2018;28(6):436–53.
16 Calcinotto A, Kohli J, Zagato E, Pellegrini L, Demaria M, Alimonti A. Cellular senescence: aging, cancer, and injury. Physiol Rev. 2019;99(2):1047–78.
17 Regulski MJ. Cellular senescence: what, why, and how. Wounds. 2017;29(6):168–74.
18 Zhu M, Meng P, Ling X, Zhou L. Advancements in therapeutic drugs targeting of senescence. Ther Adv Chronic Dis. 2020;11:2040622320964125.
19 Mohamad Kamal NS, Safuan S, Shamsuddin S, Foroozandeh P. Aging of the cells: insight into cellular senescence and detection methods. Eur J Cell Biol. 2020;99(6):151108.
20 Kowald A, Passos JF, Kirkwood TBL. On the evolution of cellular senescence. Aging Cell. 2020;19(12):e13270.

21 Kritsilis M, V Rizou S, Koutsoudaki PN, Evangelou K, Gorgoulis VG, Papadopoulos D. Ageing, cellular senescence and neurodegenerative disease. Int J Mol Sci. 2018;19(10):E2937.
22 Zhou L, Li Y, Hao S, Zhou D, Tan RJ, Nie J, et al. Multiple genes of the renin-angiotensin system are novel targets of Wnt/β-catenin signaling. J Am Soc Nephrol. 2015;26(1):107–20.
23 Pez F, Lopez A, Kim M, Wands JR, Caron de Fromentel C, Merle P. Wnt signaling and hepatocarcinogenesis: molecular targets for the development of innovative anticancer drugs. J Hepatol. 2013;59(5):1107–17.
24 Li J, Sutter C, Parker DS, Blauwkamp T, Fang M, Cadigan KM. CBP/p300 are bimodal regulators of Wnt signaling. Embo J. 2007;26(9):2284–94.
25 Emami KH, Nguyen C, Ma H, Kim DH, Jeong KW, Eguchi M, et al. A small molecule inhibitor of beta-catenin/CREB-binding protein transcription [corrected]. Proc Natl Acad Sci U S A. 2004;101(34):12682–7.
26 Zhou L, Liu Y. Wnt/β-catenin signalling and podocyte dysfunction in proteinuric kidney disease. Nat Rev Nephrol. 2015;11(9):535–45.
27 Yang Y, Feng X, Liu X, Wang Y, Hu M, Cao Q, et al. Fate alteration of bone marrow-derived macrophages ameliorates kidney fibrosis in murine model of unilateral ureteral obstruction. Nephrol Dial Transplant. 2019;34(10):1657–68.
28 Qiao X, Rao P, Zhang Y, Liu L, Pang M, Wang H, et al. Redirecting TGF-beta signaling through the beta-catenin/Foxo complex prevents kidney fibrosis. J Am Soc Nephrol. 2018;29(2):557–70.
29 Essers MAG, de Vries-Smits LMM, Barker N, Polderman PE, Burgering BMT, Korswagen HC. Functional interaction between beta-catenin and FOXO in oxidative stress signaling. Science. 2005;308(5725):1181–4.
30 Stamos JL, Weis WI. The beta-catenin destruction complex. Cold Spring Harb Perspect Biol. 2013;5(1):a007898.
31 Nong J, Kang K, Shi Q, Zhu X, Tao Q, Chen YG. Phase separation of axin organizes the beta-catenin destruction complex. J Cell Biol. 2021;220(4):e202012112.
32 Aberle H, Bauer A, Stappert J, Kispert A, Kemler R. Beta-catenin is a target for the ubiquitin-proteasome pathway. Embo J. 1997;16(13):3797–804.
33 Schunk SJ, Floege J, Fliser D, Speer T. WNT-beta-catenin signalling: a versatile player in kidney injury and repair. Nat Rev Nephrol. 2021;17(3):172–84.
34 Cha PH, Cho YH, Lee SK, Lee J, Jeong WJ, Moon BS, et al. Small-molecule binding of the axin RGS domain promotes beta-catenin and Ras degradation. Nat Chem Biol. 2016;12(8):593–600.
35 Racusen LC, Monteil C, Sgrignoli A, Lucskay M, Marouillat S, Rhim JG, et al. Cell lines with extended in vitro growth potential from human renal proximal tubule: characterization, response to inducers, and comparison with established cell lines. J Lab Clin Med. 1997;129(3):318–29.
36 Beard JR, Bloom DE. Towards a comprehensive public health response to population ageing. Lancet. 2015;385(9968):658–61.
37 Nabavi SF, Braidy N, Habtemariam S, Sureda A, Manayi A, Nabavi SM. Neuroprotective effects of fisetin in Alzheimer's and Parkinson's diseases: from chemistry to medicine. Curr Top Med Chem. 2016;16(17):1910–5.
38 Chen Y, Pu Q, Ma Y, Zhang H, Ye T, Zhao C, et al. Aging reprograms the hematopoietic-vascular niche to impede regeneration and promote fibrosis. Cell Metab. 2021;33(2):395–410.e4.
39 Wan J, Wu X, Chen H, Xia X, Song X, Chen S, et al. Aging-induced aberrant RAGE/PPARα axis promotes hepatic steatosis via dysfunctional mitochondrial β oxidation. Aging Cell. 2020;19(10):e13238.
40 Fuchs MAA, Broeker KAE, Schrankl J, Burzlaff N, Willam C, Wagner C, et al. Inhibition of transforming growth factor β1 signaling in resident interstitial cells attenuates profibrotic gene expression and preserves erythropoietin production during experimental kidney fibrosis in mice. Kidney Int. 2021;100(1):122–37.
41 Minutolo R, Borrelli S, De Nicola L. CKD in the elderly: kidney senescence or blood pressure-related nephropathy? Am J Kidney Dis. 2015;66(2):184–6.
42 Bogdanova E, Beresneva O, Galkina O, Zubina I, Ivanova G, Parastaeva M, et al. Myocardial hypertrophy and fibrosis are associated with cardiomyocyte beta-catenin and TRPC6/Calcineurin/NFAT signaling in spontaneously hypertensive rats with 5/6 nephrectomy. Int J Mol Sci. 2021;22(9):4645.
43 Xiang FL, Fang M, Yutzey KE. Loss of beta-catenin in resident cardiac fibroblasts attenuates fibrosis induced by pressure overload in mice. Nat Commun. 2017;8(1):712.
44 Tokunaga Y, Osawa Y, Ohtsuki T, Hayashi Y, Yamaji K, Yamane D, et al. Selective inhibitor of Wnt/β-catenin/CBP signaling ameliorates hepatitis C virus-induced liver fibrosis in mouse model. Sci Rep. 2017;7(1):325.
45 Nishikawa K, Osawa Y, Kimura K. Wnt/β-catenin signaling as a potential target for the treatment of liver cirrhosis using antifibrotic drugs. Int J Mol Sci. 2018;19(10):E3103.
46 Cao H, Wang C, Chen X, Hou J, Xiang Z, Shen Y, et al. Inhibition of Wnt/β-catenin signaling suppresses myofibroblast differentiation of lung resident mesenchymal stem cells and pulmonary fibrosis. Sci Rep. 2018;8(1):13644.
47 Okazaki H, Sato S, Koyama K, Morizumi S, Abe S, Azuma M, et al. The novel inhibitor PRI-724 for Wnt/β-catenin/CBP signaling ameliorates bleomycin-induced pulmonary fibrosis in mice. Exp Lung Res. 2019;45(7):188–99.
48 Rao P, Pang M, Qiao X, Yu H, Wang H, Yang Y, et al. Promotion of beta-catenin/Foxo1 signaling ameliorates renal interstitial fibrosis. Lab Invest. 2019;99(11):1689–701.
49 Martins R, Lithgow GJ, Link W. Long live FOXO: unraveling the role of FOXO proteins in aging and longevity. Aging Cell. 2016;15(2):196–207.
50 Baar MP, Brandt RMC, Putavet DA, Klein JDD, Derks KWJ, Bourgeois BRM, et al. Targeted apoptosis of senescent cells restores tissue homeostasis in response to chemotoxicity and aging. Cell. 2017;169(1):132–47.e16.
51 Kim DH, Lee B, Lee J, Kim ME, Lee JS, Chung JH, et al. FoxO6-mediated IL-1β induces hepatic insulin resistance and age-related inflammation via the TF/PAR2 pathway in aging and diabetic mice. Redox Biol. 2019;24:101184.
52 Chung SY, Huang WC, Su CW, Lee KW, Chi HC, Lin CT, et al. FoxO6 and PGC-1α form a regulatory loop in myogenic cells. Biosci Rep. 2013;33(3):e00045.
53 Zhou L, Chen X, Lu M, Wu Q, Yuan Q, Hu C, et al. Wnt/β-catenin links oxidative stress to podocyte injury and proteinuria. Kidney Int. 2019;95(4):830–45.
54 Zhou L, Mo H, Miao J, Zhou D, Tan RJ, Hou FF, et al. Klotho ameliorates kidney injury and fibrosis and normalizes blood pressure by targeting the renin-angiotensin system. Am J Pathol. 2015;185(12):3211–23.